



UNIVERSITAT DE
BARCELONA

Caracterización del vulcanismo carbonatítico de Catanda (Angola)

Marc Campeny Crego

ADVERTIMENT. La consulta d'aquesta tesi queda condicionada a l'acceptació de les següents condicions d'ús: La difusió d'aquesta tesi per mitjà del servei TDX (www.tdx.cat) i a través del Dipòsit Digital de la UB (deposit.ub.edu) ha estat autoritzada pels titulars dels drets de propietat intel·lectual únicament per a usos privats emmarcats en activitats d'investigació i docència. No s'autoritza la seva reproducció amb finalitats de lucre ni la seva difusió i posada a disposició des d'un lloc aliè al servei TDX ni al Dipòsit Digital de la UB. No s'autoritza la presentació del seu contingut en una finestra o marc aliè a TDX o al Dipòsit Digital de la UB (framing). Aquesta reserva de drets afecta tant al resum de presentació de la tesi com als seus continguts. En la utilització o cita de parts de la tesi és obligat indicar el nom de la persona autora.

ADVERTENCIA. La consulta de esta tesis queda condicionada a la aceptación de las siguientes condiciones de uso: La difusión de esta tesis por medio del servicio TDR (www.tdx.cat) y a través del Repositorio Digital de la UB (deposit.ub.edu) ha sido autorizada por los titulares de los derechos de propiedad intelectual únicamente para usos privados enmarcados en actividades de investigación y docencia. No se autoriza su reproducción con finalidades de lucro ni su difusión y puesta a disposición desde un sitio ajeno al servicio TDR o al Repositorio Digital de la UB. No se autoriza la presentación de su contenido en una ventana o marco ajeno a TDR o al Repositorio Digital de la UB (framing). Esta reserva de derechos afecta tanto al resumen de presentación de la tesis como a sus contenidos. En la utilización o cita de partes de la tesis es obligado indicar el nombre de la persona autora.

WARNING. On having consulted this thesis you're accepting the following use conditions: Spreading this thesis by the TDX (www.tdx.cat) service and by the UB Digital Repository (deposit.ub.edu) has been authorized by the titular of the intellectual property rights only for private uses placed in investigation and teaching activities. Reproduction with lucrative aims is not authorized nor its spreading and availability from a site foreign to the TDX service or to the UB Digital Repository. Introducing its content in a window or frame foreign to the TDX service or to the UB Digital Repository is not authorized (framing). Those rights affect to the presentation summary of the thesis as well as to its contents. In the using or citation of parts of the thesis it's obliged to indicate the name of the author.

Publicaciones originales

9.4. Publicación IV

Campeny M., Kamenetsky, V.S., Melgarejo J.C., Giuliani, A., Maas, R., Kohn, B., Matchan, E., Mangas J., Manuel J., Gonálves A.O. (2015): Incipient rifting in the West African margin manifested by recent carbonatitic volcanism in Catanda (Angola).

Incipient continental rifting in SW Africa manifested by recent carbonatitic volcanism in Angola

M Campeny¹, VS Kamenetsky², JC Melgarejo¹, A Giuliani³, R Maas³, B Kohn³, E Matchan³, J Mangas⁴, J Manuel⁵, AO Gonçalves⁵

¹Departament de Cristal·lografia, Mineralogia i Dipòsits Minerals, Universitat de Barcelona

²School of Physical Sciences, University of Tasmania, Hobart, Tasmania, Australia

³School of Earth Sciences, University of Melbourne, Melbourne, Victoria, Australia

⁴Departamento de Física, Instituto de Oceanografía y Cambio Global, Univ. Las Palmas de Gran Canaria

⁵Departamento de Geología, Universidade Agostinho Neto, Luanda, Angola.

Abstract

The continental lithosphere thinning generate elongated depressions known as continental rifts, those are instability regions where continents can be pulled apart. Incipient rifting stages are represented by the emplacement of alkaline magmas, such as carbonatites – composed of >50% of carbonates. Carbonatitic volcanism was reported in the Catanda area (Angola). Their age was estimated to be Cretaceous, i.e. similar to other magmatic activity of kimberlites and carbonatites in central and eastern. The Angolan carbonatites and kimberlites are distributed along a narrow (1000 km wide) SW-NE trending depression, the Lucapa corridor. Here we report new $^{40}\text{Ar}/^{39}\text{Ar}$ and (U-Th-Sm)/He geochronology results on phlogopite and fluorapatite, which demonstrate that the Catanda carbonatites were emplaced at 0.65 ± 0.05 Ma. Seismic tomography evidences a low-velocity zone beneath Catanda and extending towards inland Angola, proving the occurrence of upper-mantle magmatism beneath this area. $\epsilon\text{Hf}-\epsilon\text{Nd}$ isotopic values obtained in Catanda are similar to those reported for mantle-derived melts (i.e. OIB's and Group I Kimberlites) and Sr-Nd isotopes present similitudes to carbonatites from continental rifting areas worldwide. Our dating and isotopic data, combined with the geophysical evidence suggest that the Catanda volcanism was inextricably linked to the present-day re-activation of the Lucapa rift. Lucapa were relevant in the break-up of Gondwana during the Cretaceous so it is not discernable that Africa can break up along this rifting structure in the future. At last, considering the young age of the Catanda volcanism, the occurrence of upcoming carbonatitic eruptions in this region of SW Africa is also plausible.

Keywords: continental rifting, carbonatites, Lucapa, Catanda, Angola

1. Introduction

Rifting events are extensional processes associated to asthenosphere rising and the corresponding thinning of the overlying lithosphere. In continental areas, these processes may create instability regions where continents can be pulled apart and even generate new plate boundaries, in the last stages of rifting evolution (Fourel et al., 2013). The incipient stages of rifting are associated with the emplacement of alkaline and carbonatite magmas in the crust (Pirajno, 2015). Several examples of incipient rifting areas with associated alkaline-carbonatite magmatism have been reported worldwide as, for example, the Rio Grande rise (Brasil) (O'Connor & Duncan, 1990), the Cenozoic European Rift System (CERS) (Lustrino & Wilson, 2007) or the East African Rift (EAR) (Chorowicz, 2005).

In the west margin of Africa is located the Lucapa corridor (Fig.1), a >1000 km-long NE-SW graben defined by a set of discontinuous fractures along. The Lucapa structure is located along the suture of Pan-African belts; those were originated during Neoproterozoic orogenic events in relation to the formation of the Gondwana supercontinent (McKenzie, 2015). Magmatism in Lucapa has been intermittent, occurring in the Neoproterozoic and the Permian (Sykes, 1978) and latter in the Cretaceous, when kimberlites, carbonatites and related magmas emplaced in the upper crust, which is probably best represented by the age of several kimberlite localities such as Catoca (117.9 ± 0.7 Ma) (Robles-Cruz et al., 2012), Val do Queve (133.4 ± 11.5 Ma) (Haggerty et al., 1983) or Luxinga clusters (from 145 to 113 Ma) (Eley et al., 2008). During the Cretaceous, Lucapa structures also played a relevant role in the break-up of Gondwana and the corresponding opening of the Atlantic Ocean. Nowadays, the Lucapa corridor is approximately aligned to the Rio Grande Atlantic fracture zone (Fig.1), which is considered the boundary between the Central and the Southern segments of the Atlantic Ocean (Moulin et al., 2010), so, now, the main question is if Western Africa can break up along this seemingly inter-continental structure.

Volcanic activity in the Lucapa corridor is well represented in the northern border of the area by the Catanda extrusive carbonatites (Fig.1). The Catanda carbonatite complex consists of a cluster of small volcanic edifices with maar and tuff ring morphologies that outcrop over a 50-km² area hosted in Archaean granites (Campeny et al., 2014). The volcanic materials are mainly pyroclastic rocks but also minor carbonatitic lavas are found, which include altered natrocarbonatites (Campeny et al., 2015), similar to those reported in few localities from the EAR such as the Oldoinyo Lengai, Tinderet or Kerimasi (Hay, 1983; Deans & Roberts, 1984; Dawson, 1993; Zaitsev et al., 2013). Some nephelinitic dykes are also present in the Catanda area and a poorly constrained K-Ar age of 92 ±7 Ma was reported for one of these dykes (Torquato & Amaral, 1973). A similar age was also proposed for the carbonatite rocks (Silva & Pereira, 1973). However, the well-preserved morphology of the volcanic edifices and present-day hydrothermal activity (i.e. travertine deposits, mud-spots) in the area suggest a younger age for the carbonatites (Fig. 2). Here, we present the first direct dating of the Catanda carbonatites, which indicate a Middle Pleistocene age for this volcanism. This new dating argues for the present-day magmatic re-activation of rifting structures from the Lucapa corridor. The general implications of this new finding are discussed below.

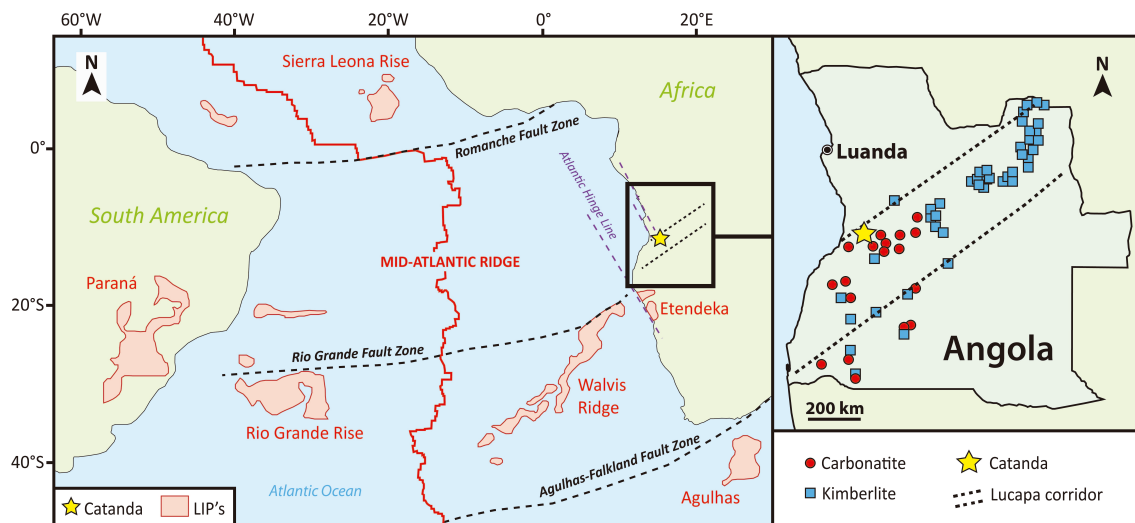


Figure 1. Synthetic map of the Mid-Atlantic Ridge. Location of the Catanda volcanic carbonatites and the Lucapa rift domain in relation to the tectonic structures and magmatic regions of the Mid-Atlantic Ridge area. Map of distribution of main carbonatites and kimberlites located in Angola.

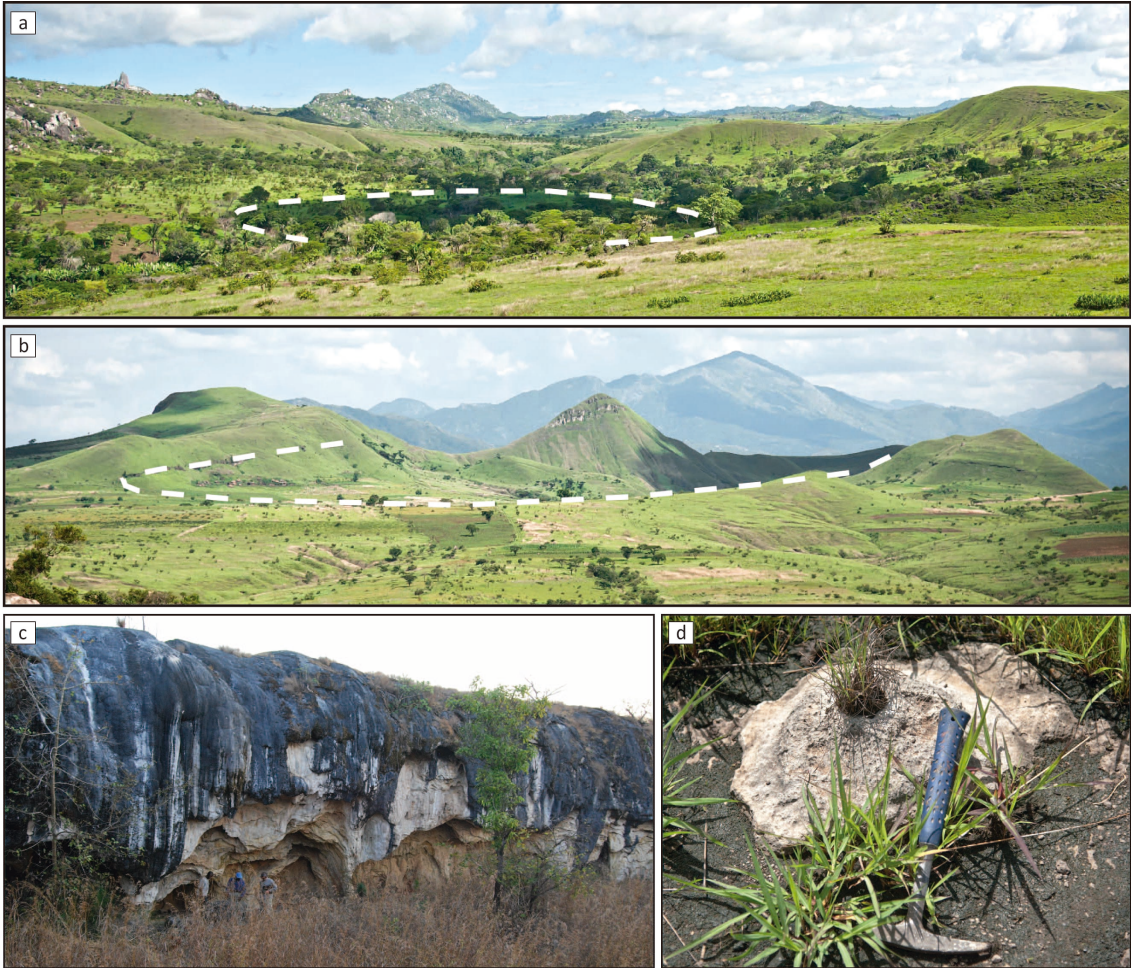


Figure 2. Detailed images from the Catanda area outcrops. (a), (b) General view of Catanda volcanic edifices in which is possible to distinguish a well-preserved morphology of the eruptive centres. (c) Travertine deposits up to 30 m thick, associated to present-day hydrothermal systems located in the Catanda area. (d) Recent carbonated mud pots in the carbonatite outcrops from Catanda.

2. Results

Catanda volcanic series mainly consist of pyroclastic rocks, those are generated during explosive eruptive episodes and contain carbonatitic minerals but also several grains coming from the hosted Archaean granites (Campeny et al., 2014). Given this consideration, our work has been focused in the study of the minor Catanda carbonatitic lavas, generated during more effusive episodes and majorly composed by primary carbonatitic minerals without a significant percentage xenolithic material. Catanda lavas generally consist of variable proportions of microphenocrysts of calcite, fluorapatite, magnetite, clinopyroxene and phlogopite hosted in calcite-rich groundmass also composed by variable proportion of accessory minerals such as

pyrochlore, perovskite, cuspidine and periclase (Campeny et al., 2015). We calculated the age of the Catanda carbonatites through ^{40}Ar - ^{39}Ar dating of phlogopite (556 ± 21 ka) and (U-Th-Sm)/He dating of fluorapatite (660 ± 90 ka) at the University of Melbourne (see Methods). The Sr-Nd-Hf-Pb isotopic compositions of fluorapatite and clinopyroxene grains from lava samples of three distinct units were also measured at the University of Melbourne (see Methods) (Table. A6). Catanda isotopic values are similar to those described in other present-day volcanic carbonatites associated to continental rift areas worldwide (Fig.3), such as the Quaternary carbonatites from the EAR (Bell & Blenkinsop, 1987) and the Eifel volcanoes, those are located in the CERS (Riley et al., 1996).

3. Methods

3.1. U-Pb dating of fluorapatite

Fluorapatite is one of the most abundant minerals in the Catanda rocks, but attempts to date fluorapatite by laser ablation ICP-MS were unsuccessful. We analysed 60 fluorapatite grains, and despite promising U and Th concentrations (1.8 to 14.6 ppm of U and 16.9 to 232.3 ppm of Th; Table. A1), $^{207}/^{206}\text{Pb}$ ratios are high (0.78 to 1.02; Table. A2) and dominated by “common Pb” (i.e. non-radiogenic Pb incorporated in the mineral lattice during crystallisation) and do not show clear correlations with $^{238}\text{U}/^{206}\text{Pb}$ ratios in the Tera-Wasserburg diagram. Pb isotope data for one fluorapatite (#21) and the groundmass samples for 3 samples (#21, #24, #25) acquired by MC-ICPMS (with U/Pb and Th/Pb from trace element data for the same sample solutions; Table. A1), also failed to provide unequivocal age information. Despite high and variable $^{238}\text{U}/^{204}\text{Pb}$ (120-314) and $^{232}\text{Th}/^{204}\text{Pb}$ (354-3585), measured $^{206}\text{Pb}/^{204}\text{Pb}$ and $^{208}\text{Pb}/^{204}\text{Pb}$ ratios are similarly low in all 4 fractions (20.09-20.58, 39.87-40.18) (Table. A2). In the Th-Pb isochron diagram, the data points for the groundmass samples define a well-correlated line (MSWD 0.67, 2σ input errors of $x=1\%$, $y=0.1\%$, $\rho=0.6$) with an apparent age of 10.3 ± 1.8 Ma ($^{208}\text{Pb}/^{204}\text{Pb}_{\text{i}}=39.69 \pm 6$). By contrast, the Th-Pb data for fluorapatite and groundmass in sample #21 yield an apparent age of 1.26 ± 0.36 Ma

($^{208}\text{Pb}/^{204}\text{Pb}=39.96\pm 5$). In summary, the ^{238}U - ^{206}Pb system does not yield interpretable age constraints.

3.2. (U-Th-Sm)/He dating of fluorapatite

Nine different grains of fluorapatite from two different carbonatitic lava samples were used for (U-Th-Sm)/He (AHe) analysis. The method used followed an established laboratory routine for laser He extraction (House et al., 2000). Whereas clear euhedral and non-fractured grains are usually sought for such analysis, in this case all crystals were markedly anhedral and fractured. Grains chosen for analysis were hand picked under an Olympus SZX12 binocular microscope and subsequently immersed in ethanol and checked under polarised light to detect possible mineral inclusions. As it was not possible to accurately estimate the grain geometry for applying the α -ejection correction (Farley et al., 1996), grains selected were subjected to mechanical air abrasion. This was achieved by using silicon carbide grit (300-425 μm) to remove at least the outer ~ 25 - $30 \mu\text{m}$ of the apatite ($> \alpha$ -ejection distance) in a cell similar to that described by Krogh (1982). This approach has previously been applied to (U-Th)/He dating of Late Tertiary to Quaternary volcanic samples (Spiegel et al., 2009). Abrasion was halted periodically and grain sizes and shapes were monitored using digital image capture. Using this approach makes it unnecessary to apply the α -ejection correction, and can also potentially overcome any influence of He implantation into the apatite from surrounding minerals.

In order to extract sufficient ^4He gas for measurement for most analyses more than one grain was required and these were loaded into small, acid-treated platinum capsules. Grains were then outgassed under vacuum at $\sim 900^\circ\text{C}$ for 5 minutes, using a semiconductor diode Coherent Quattro FAP laser, set on a wavelength of 820 nm with fibre-optic coupling to the sample chamber (to provide optimal coupling with samples and heating without melting, ablation or fusion). ^4He content was determined by isotope dilution using a pure ^3He spike calibrated against an independent ^4He standard and measured using a Balzers quadrupole (QMS 200–Prisma) mass spectrometer. A hot blank was run after each gas extraction to verify complete outgassing of the apatite grains. Most samples yielded negligible amounts of gas even after the first re-

extract, and for all samples the second re-extract contributed less than 0.5% of the total measured ^4He .

Samples were removed from the laser chamber and ^{238}U , ^{235}U , ^{232}Th and ^{147}Sm concentrations obtained by total dissolution of outgassed fluorapatite (still in their Pt capsules) in HNO_3 and analysed using an Agilent 7700x inductively coupled plasma mass spectrometer (ICP-MS). Analyses were calibrated using the reference material BHVO-1, with Mud Tank apatite and international rock standard BCR-2 used as check standards and run together with each batch of samples analysed. Analytical uncertainties for the University of Melbourne He facility for abraded samples (where uncertainties in grain size measurements do not need to be taken into account) are estimated at 3% ($\pm 1\sigma$), which incorporates gas analysis and ICP-MS analytical uncertainties. Accuracy and precision of U, Th and Sm content ranges up to 2% (at $\pm 2\sigma$), but is typically better than 1%. With each batch of samples analysed Durango apatite was also run as an internal standard and served as a further check on accuracy. The weighted mean of 4 Durango apatite measurements carried out for this study was 31.2 ± 1.9 Ma (uncertainty at 95% confidence level). This compares favourably (within error uncertainties) with a (U-Th-Sm)/He age of 31.02 ± 1.01 Ma ($\pm 1\sigma$) reported for a set of 24 Durango apatite analyses carried in the Caltech He laboratory. The results obtained for the two samples yield grand weighted apparent ages of 650 ± 130 ka and 660 ± 90 ka ($\pm 2\sigma$), respectively (Table. A3).

3.3. Rb-Sr dating of phlogopite

Phlogopite is also a common microphenocryst in all Catanda carbonatite lavas. Preliminary trace element data for phlogopite from 3 samples (PHL-21, PHL-24, PHL-25) indicated high Sr contents (200-4000 ppm) and $\text{Rb/Sr} < 1$, presumably related to Sr-rich impurities (fluorapatite, carbonate) (Table. A4). Two splits of each separate were therefore briefly leached with warm 0.5M and 2M nitric acid, respectively, to gently remove easily soluble impurities and generate higher Rb/Sr ratios – more suitable for Rb-Sr dating - in the residual phlogopite (Maas, 2003). This treatment reduced Sr contents to 115-227 ppm and raised Rb/Sr to 1.79-4.48. The complementary 2M nitric acid leachates were high in Sr and had low Rb/Sr (0.05-0.28). Measured $^{87}\text{Sr}/^{86}\text{Sr}$ in the

phlogopite residues is low (0.70331-0.70397; Table. A4), irrespective of Rb/Sr, and similar to measured $^{87}\text{Sr}/^{86}\text{Sr}$ in the leachates (0.70346-0.70348; Table. A4) and in coexisting fluorapatite and clinopyroxene (0.70309-0.70354; Table. A4). This suggests that the Rb-Sr systems are very young. Various combinations of data points yield apparent ages in the range 0-4 Ma but no firm conclusions can be drawn because the data do not produce clear isochronous arrays.

3.4. $^{40}\text{Ar}-^{39}\text{Ar}$ dating of phlogopite

Five phlogopite grains from samples PHL-21, PHL-24 and PHL-25 were also analysed for $^{40}\text{Ar}/^{39}\text{Ar}$ dating with a new generation ARGUSVI mass spectrometer (Phillips & Matchan, 2014) Samples PHL-24 and PHL-25 behaved quite similarly to one another, and contained a higher proportion of $^{40}\text{Ar}^*$ (~15% of total ^{40}Ar) (Table. A5). Total gas ages ranged from 582 ± 26 ka to 797 ± 80 ka. Data points were combined for inverse isochron analysis, which reveals the presence of some excess argon in these grains ($^{40}\text{Ar}/^{36}\text{Ar} = 302.2 \pm 1.1$ during 2σ). The 6-pt inverse isochrone age yield 556 ± 21 ka (2σ), derived from combining high-T data from PHL-24 and PHL-25. On the other hand, sample PHL-21 was collected from underlying stratigraphic compared to samples PHL-24 and PHL-25, and this fact is also reflected in the significant older age. Calculating a weighted mean age from concordant $^{40}\text{Ar}^*/^{39}\text{Ar}$ values from high-T heating steps (from all five grains, n=7 steps), sample PHL-21 yields an age of 741 ± 44 ka (6% 2σ ; MSWD = 1.3, p=0.23; Table. A5).

3.5. Sr-Nd-Pb-Hf isotopes

Fluorapatite and clinopyroxene from samples 21, 24 and 25 show variable Sr contents (3539-4274 ppm in fluorapatite, 147-2861 ppm in clinopyroxene), low Rb/Sr ($^{87}\text{Rb}/^{86}\text{Sr}$ 0.00003-0.00045 in fluorapatite, 0.0059-0.096 in clinopyroxene) and a narrow range of measured $^{87}\text{Sr}/^{86}\text{Sr}$ (0.70309-0.70354) (Table. A6). Nd concentrations are similarly diverse (536-1155 ppm in fluorapatite, 16.3-40.6 ppm in clinopyroxene, 183-220 ppm in groundmass) but measured $^{143}\text{Nd}/^{144}\text{Nd}$ ratios show little range (0.512782-0.512855, eNd +2.1 to +4.2, average $+3.0 \pm 0.6$, 1s). $^{176}\text{Hf}/^{177}\text{Hf}$ ratios for groundmass and

clinopyroxene also show a narrow range (0.282752-0.282827, eHf -0.7 to +1.9), as do the Pb isotope ratios for the groundmass and one of the fluorapatite fractions (Table A6). Given the young age of the carbonatite, age corrections are trivial in almost all cases ($^{208}\text{Pb}/^{204}\text{Pb}$ in 21ap shifts from 40.18 to 40.06).

4. Discussion

The Middle Pleistocene age obtained for the Catanda carbonatites indicates active volcanism in SW Angola. Recent low magnitude earthquakes (4.2 to 5.1 M; <http://www.earthquake.usgs.gov>) of unresolved focal mechanism in the area also points to active tectonism along this region. Modern tectonics is also represented by a Quaternary transform faults system known as the Atlantic Hinge Line (Guiraud et al., 2010), which is sub-parallel to the Angolan coastline and the Mid-Atlantic Ridge (Fig.1). So, the main question is whether this volcanic and tectonic activity at Catanda is due to a local anomaly or can be linked to a broader-scale tectonic process.

The broad-scale option is supported by seismic tomography studies; those reported a low-velocity region at the lithosphere-asthenosphere boundary beneath the Catanda area and extending towards inland Angola (Fishwick, 2010; Hansen 2012). This mantle anomaly is also complemented by the detection of anomalous positive topography in the same area (Moucha & Forte, 2011). The ϵ Hf- ϵ Nd isotopic relation obtained for the Catanda lavas agree with the lithosphere-asthenosphere origin for the Catanda parental melts, plotting well below the global Hf-Nd isotope array and being also similar to geochemical signature of mantle-derived magmas such as the OIB's and the Group I kimberlites (Fig. 3a).

Similar low velocity regions and topographic anomalies as detected in SW Angola have been reported in incipient continental rift areas worldwide, such as the EAR (Pik, 2011; Civiero, 2015) or the CERS (Ritter et al., 2001; Wüllner et al., 2006), where the occurrence of volcanic events of carbonatitic composition is also well known (Woolley & Church, 2005).

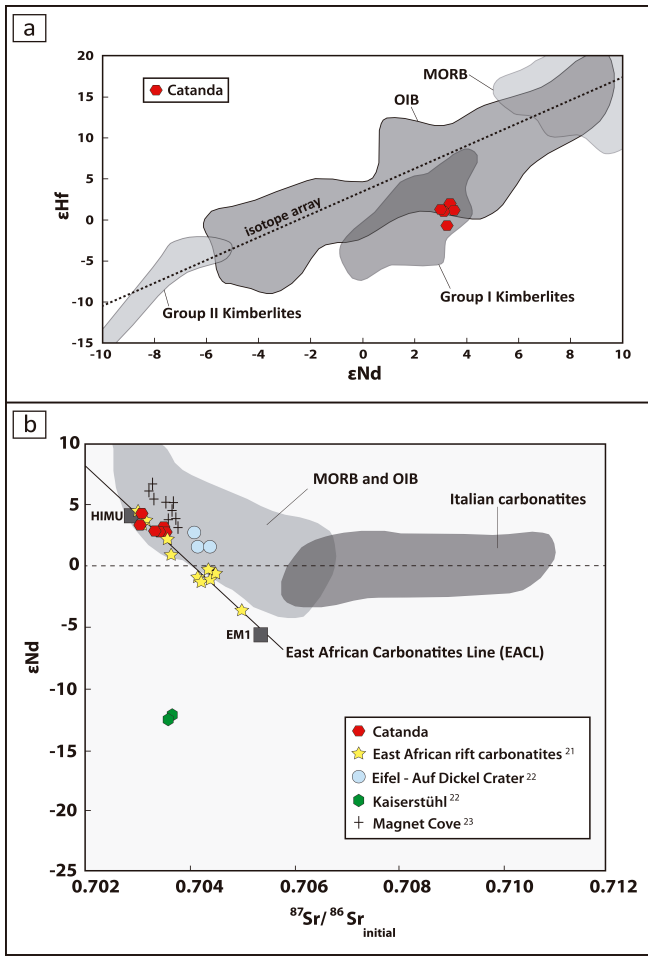


Figure 3. Covariation of Sr-Nd and Nd-Hf isotopic compositions. (a) Comparison of the Catanda carbonatites Sr-Nd isotope composition between global data set from carbonatites worldwide. (b) Nd-Hf composition of Catanda carbonatites compared to the oceanic basalts composition and to the Group I and Group II kimberlites.

The similitudes of Catanda with worldwide incipient continental rift areas is also supported by the occurrence of altered natrocarbonatite lavas (Campeny et al., 2015), similar to those described in a few localities from the EAR (i.e. Kerimasi and Tinderet: Hay, 1983; Deans & Roberts, 1984; Zaitsev & Keller, 2006; Zaitsev et al., 2013) and the CERS (i.e. Rockeskyll complex; Keller, 1989; Riley et al., 1996). The Sr-Nd isotopic features of the Catanda lavas confirm this resemblance. Catanda data follow the trend marked by the volcanic carbonatite localities from the EAR and also present like values to those reported in the Eifel carbonatites (Fig. 3b).

In our opinion, the occurrence of mantle geophysical anomalies in the area, the isotopic and compositional features of the Catanda lavas and the general similitudes between Catanda and incipient continental rift areas with associated carbonatitic

volcanism worldwide (i.e. the EAR and the CERS) argue for the occurrence of a broad-scale process of embryonic rifting in SW Angola.

The more plausible option to explain the origin of this process is the re-activation of the Lucapa rift structures, where the majority of the Angolan kimberlites and carbonatites, including Catanda, stand out (Fig.1). The Lucapa corridor was formed with the Pan-African orogen (at about 500-550 Ma) and the corridor experienced intermittent periods of extensional tectonism and anorogenic magmatism since the Neoproterozoic and later at the Permian and Cretaceous (Sykes, 1978; Jelsma et al., 2009). Anorogenic magmatism is well characterized by the intermittence of tectonic relaxed periods and apparent quiescence (Martin et al., 2012) as seems that occurred in Lucapa and also in several localities worldwide, those are associated with alkaline or carbonatitic magmatism such as in Chilwa (Malawi), Gardar (Greenland), Kola (Russia), or Grenville (Canada) (Martin et al., 2012). Following the intermittence of these cycles, it seems that Lucapa corridor is nowadays suffering a new period of magmatic re-activation, but the main issue is to understand why this process is occurring in this region at present-day.

A very plausible answer is the existence of a deep mantle superplume beneath Southern Africa (Gurnis, 2000), which has continuity to the upper mantle and contributes to the generation of shallow magmatic events (Al Hajri et al., 2009). The interaction of this superplume is broadly accepted to explain the magmatism of the EAR (Ritsema et al., 1999; Behn 2004; Civiero, 2015), but recent works argue for its displacement towards western Africa (Conrad, 2003). Then, would be not discernable the connection of this lower mantle superplume with the occurrence of embryonic continental rifting in SW Africa, which would be exemplified by the Pleistocene carbonatitic volcanism at the Catanda area.

In summary, our general interpretation is that present-day embryonic sub-lithospheric rifting is nowadays occurring in SW Africa. This process would be related with tectonic and magmatic re-activation of the Lucapa rift structures, generated by the interaction of the southern African superplume with the upper mantle beneath western Angola.

This general setting is exemplified by the occurrence of carbonatitic volcanism in the Catanda region.

The Lucapa rift structures were relevant in the break-up of Gondwana and the corresponding opening of the Atlantic Ocean during the Cretaceous so should not be discarded that western Africa can break up along this inter-continental structure if the rifting process continues active in the future.

At last, considering the young age of the Catanda volcanism, and the profusion of carbonatite and kimberlite outcrops in the Lucapa corridor, the occurrence of future alkaline-carbonatitic or kimberlitic eruptions in this portion of SW Africa is also plausible.

Acknowledgements

The consolidated research group SGR-444 of the Catalonia's government, the research project CGL2009-13758 of the Spanish Government and the Australian Research Council, have supported the present work. The University of Melbourne geochronology facilities receives infrastructure support from the National Collaborative Research Infrastructure Strategy AuScope program and the Education Investment Fund AGOS program. Logistics have been funded by the Hugh E. McKinstry fund, granted by the Society of Economic Geologists (SEG). We would also like to thank the collaboration during the fieldwork of José Fortuna and Felipe Correia from the Catanda village.

References

- Al Hajri Y, White N, Fishwick S (2009) Scales of transient convective support beneath Africa. *Geology* 37(10): 883–886.
- Behn M, Conrad CP, Silver PG (2004) Detection of upper mantle flow associated with the African Superplume. *Earth and Planetary Science Letters* 224: 259–274.
- Bell K, Blenkinsop J (1987) Nd and Sr isotopic compositions of East African carbonatites: Implications for mantle heterogeneity. *Geology* 15(2): 99–102.
- Campeny M, Mangas J, Melgarejo JC, Bambi A, Alfonso P, Manuel J (2014) The Catanda extrusive carbonatites (Kwanza Sul, Angola): an example of explosive carbonatitic volcanism. *Bulletin of Volcanology* 76: 818–832.
- Campeny M, Kamenetsky VS, Melgarejo JC, Mangas J, Manuel J, Alfonso P, Kamenetsky MB, Bambi A, Gonçalves AO (2015) Carbonatitic lavas in Catanda (Kwanza Sul, Angola): mineralogical and geochemical constraints on the parental melt. *Lithos* 232: 1–11.
- Chorowicz J (2005) The East African Rift system. *Journal of African Earth Sciences* 43: 379–410.
- Civiero C, Hammond JOS, Goes S, Fishwick S, Ahmed A, et al. (2015) Multiple mantle upwellings in the transition zone beneath the northern East-African Rift system from relative P-wave travel-time tomography. *Geochemistry, Geophysics, Geosystems* 16: 2949–2968.
- Conrad CP, Gurnis M (2003) Seismic tomography, surface uplift, and the breakup of Gondwanaland: Integrating mantle convection backwards in time. *Geochemistry, Geophysics, Geosystems* 4(3): 1031.

Dawson JB (1993) A supposed sövite from Oldoinyo Lengai, Tanzania: result of extreme alteration of alkali carbonatite lava. *Mineralogical Magazine* 57: 93–101.

Deans T, Roberts B (1984) Carbonatite tuffs and lava clasts of the Tinderet foothills, western Kenya: a study of calcified natrocarbonatites. *Journal of the Geological Society of London* 141: 563–580.

Eley R, Grüter H, Louw A, Tunguno C, Twidale J (2008) Exploration Geology of the Luxinga kimberlite Cluster (Angola) with evidence supporting the presence of kimberlite lava. *Extended Abstr. No. 9IKC-A-00166, 9th Int. Kimberlite Conf., Frankfurt*.

Farley KA, Wolf RA, Silver LT (1996) The effects of long alpha-stopping distances on (U-Th)/ He ages. *Geochimica et Cosmochimica Acta* 60: 4223–4229.

Fishwick S (2010) Surface wave tomography: Imaging of the lithosphere asthenosphere boundary beneath central and southern Africa?. *Lithos* 120: 63 –73.

Fourel L, Milelli L, Jaupart C, Limare A (2013) Generation of continental rifts, basins and swells by lithosphere instabilities. *Journal of Geophysical Research-Solid Earth* 118: 1–21.

Guiraud M, Buta-Neto M, Quesne D (2010) Segmentation and differential post-rift uplift at the Angola margin as recorded by the transform-rifted Benguela and oblique-to-orthogonal-rifted Kwanza basins. *Marine and Petroleum Geology* 27: 1040–1068.

Gurnis M, Mitrovica JX, Ritsema J, van Heijst H (2000) Constraining mantle density structure using geological evidence of surface uplift rates: The case of the African Superplume. *Geochemistry, Geophysics, Geosystems* 1: 1020.

Hansen S, Nyblade AA, Benoit MH (2012) Mantle structure beneath Africa and Arabia from adaptively parameterized P-wave tomography: Implications for the origin of Cenozoic Afro-Arabian tectonism. *Earth and Planetary Science Letters* 319-320: 23–34.

Haggerty SE, Raber E, Naeser CW (1983) Fission track dating of kimberlitic zircons. *Earth and Planetary Science Letters* 63(1): 41–50.

Hay RL (1983) Natrocarbonatite tephra of Kerimasi volcano, Tanzania. *Geology* 11: 599–602.

House MA, Farley KA, Stockli D (2000) Helium Chronometry of Apatite and Titanite Using Nd-Yag Laser Heating. *Earth and Planetary Science Letters* 183: 365–368.

Jelsma H, Barnett W, Richards S, Lister G (2009) Tectonic setting of kimberlites. *Lithos* 112S, 155–165.

Jones AP, Genge M, Carmody L (2013) Carbonate melts and Carbonatites. *Reviews in Mineralogy and Geochemistry* 75: 289–322.

Keller J (1989) Extrusive carbonatites and their significance. In: *Carbonatites: Genesis and Evolution*, ed Bell K (Unwin Hyman, London), pp. 70–88.

Krogh TE (1982) Improved accuracy of U-Pb zircon ages by the creation of more concordant systems using an air abrasion technique. *Geochimica et Cosmochimica Acta* 46: 637–649.

Lustrino M, Wilson M (2007) The Circum-Mediterranean anorogenic Cenozoic Igneous Province. *Earth-Science Reviews* 81: 1–65.

Martin R, Sokolov M, Magji SS (2012) Punctuated anorogenic magmatism. *Lithos* 152, 132–140.

Maas R (2003) Acid leaching of micas: improved Rb-Sr geochronology of disequilibrated rocks from zones of alteration and deformation. *Journal of the Virtual Explorer* 13.

McKenzie D, Daly MC, Priestley K (2015) The lithospheric structure of Pangea. *Geology* 43(9): 783–78.

Mouha R, Forte AM (2011) Changes in African topography driven by mantle convection. *Nature Geoscience* 4: 707–712.

Moulin M, Aslanian D, Unternehr P (2010) A new starting point for the South and Equatorial Atlantic Ocean. *Earth-Science Reviews* 98: 1–37.

O'Connor JM, Duncan RA (1990) Evolution of the Walvis Ridge – Rio Grande Rise hot spot system: Implications for African and South American plate motions over plumes. *Journal of Geophysical Research: Solid Earth* 95: 17475–17502.

Olsen KH (1995) *Continental Rifts: Evolution, Structure, Tectonics*. (Elsevier, Amsterdam).

Phillips D, Matchan E (2014) Ultra-high precision $^{40}\text{Ar}/^{39}\text{Ar}$ ages for Fish Canyon Tuff and Alder Creek Rhyolite sanidine: New dating standards required?. *Geochimica et Cosmochimica Acta* 121: 229–239.

Pik R (2011) East Africa on the rise. *Nature Geoscience* 4: 660–661.

Pirajno F (2015) Intracontinental anorogenic alkaline magmatism and carbonatites, associated mineral systems and the mantle plume connection. *Gondwana Research* 27: 1181–1216.

Riley T, Bailey K, Lloyd FE (1996) Extrusive carbonatite from the quaternary Rockeskyll Complex, West Eifel, Germany. *The Canadian Mineralogist* 34: 389–401

Ritsema J, van Heijst HJ, Woodhouse JH (1999) Complex shear wave velocity structure imaged beneath Africa and Iceland. *Science* 286: 1925–1928.

Ritter JRR, Jordan M, Christensen UR, Achauer U (2001) A mantle plume below the Eifel volcanic fields, Germany. *Earth and Planetary Science Letters* 186: 7–14.

Robles-Cruz SE, Escayola M, Jackson S, Galí S, Pervov V, Watangua M, Gonçalves A, Melgarejo JC (2012) U-Pb SHRIMP geochronology of zircon from the Catoca kimberlite, Angola: Implications for diamond exploration. *Chemical Geology* 310–311: 137–147.

Silva MVS, Pereira E (1973) Estrutura Vulcânico-Carbonatitica da Catanda (Angola). *Boletim dos Serviços de Geologia e Minas de Angola* 24: 5–14.

Spiegel C, Kohn B, Belton D, Berner Z, Gleadow A (2009) Apatite (U-Th-Sm)/He thermochronology of rapidly cooled samples: The effect of He implantation. *Earth and Planetary Science Letters* 285: 105–114.

Sykes L (1978) Intraplate seismicity, reactivation of pre-existing zones of weakness, alkaline magmatism, and other tectonism postdating continental fragmentation. *Reviews Geophysics Space Physics* 16: 621–688.

Torquato, JR, Amaral G (1973) Algumas idades K/Ar do magmatismo mesozoico de Angola e sua correlação com o correspondente do sul do Brasil. *Boletim do Instituto de Investigacão Científica de Angola* 10: 31–38.

Woolley AR, Church AA (2005) Extrusive carbonatites: A brief review. *Lithos* 85: 1–14.

Wüllner U, Christensen UR, Jordan M (2006) Joint geodynamical and seismic modelling of the Eifel plume. *Geophysical Journal International* 165: 357–372.

Zaitsev AN, Wenzel T, Venneman T, Markl G (2013) Tinderet volcano, Kenya: an altered natrocarbonatite locality?. *Mineralogical Magazine* 77(3): 213–226.

Table A1

Table A2

Fluorapatite		AP-01	AP-02	AP-03	AP-04	AP-05	AP-06	AP-07	AP-08	AP-09	AP-10	AP-11	AP-12	AP-13	AP-14	AP-15	AP-16	AP-17	AP-18	AP-19	AP-20	AP-21	AP-22	AP-23	AP-24	AP-25	AP-26	AP-27	AP-28	AP-29	AP-30	AP-31	AP-32	AP-33	AP-34	
²⁰⁸ Pb/ ²³² U		0,021	0,021	0,016	0,022	0,028	0,030	0,015	0,014	0,020	0,019	0,028	0,027	0,023	0,024	0,031	0,020	0,016	0,015	0,015	0,016	0,036	0,029	0,032	0,017	0,020	0,031	0,030	0,030	0,021	0,055	0,016	0,035			
+/-1 RSE		4,2%	4,2%	3,9%	4,0%	3,9%	5,5%	4,5%	4,9%	3,9%	4,0%	3,8%	4,2%	4,7%	4,2%	4,2%	4,1%	4,3%	4,4%	4,4%	4,4%	4,0%	4,7%	4,3%	4,3%	6,1%	6,2%	4,3%	3,3%	3,5%	3,5%	3,2%	3,9%	4,4%		
²⁰⁸ Pb/ ²⁰⁷ Tl		0,008	0,009	0,005	0,014	0,008	0,004	0,005	0,002	0,010	0,006	0,010	0,009	0,012	0,008	0,009	0,010	0,009	0,008	0,007	0,008	0,007	0,007	0,021	0,014	0,017	0,002	0,003	0,019	0,011	0,009	0,013	0,012	0,016	0,007	0,005
+/-1 RSE		23,4%	30,0%	22,4%	38,0%	21,9%	3,3%	21,8%	3,3%	33,6%	20,2%	17,1%	15,1%	19,9%	18,0%	22,2%	25,9%	33,3%	32,5%	30,8%	22,3%	28,6%	31,0%	31,8%	30,3%	4,0%	4,0%	37,6%	32,0%	19,3%	31,2%	18,1%	15,3%	37,1%	2,6%	
²⁰⁷ Po/ ²⁰⁸ Pb		0,963	0,964	0,906	0,920	0,857	0,859	0,888	0,904	0,827	0,872	0,884	0,863	0,936	0,998	0,916	0,909	1,021	0,885	0,937	0,990	0,855	1,000	0,913	0,915	0,924	0,983	0,909	0,822	0,860	0,802	0,833	0,787	0,910	0,840	
+/-1 RSE		4,6%	4,6%	4,0%	4,3%	4,0%	5,8%	4,1%	5,1%	3,9%	4,2%	3,9%	4,7%	5,7%	4,5%	4,4%	4,5%	4,0%	4,6%	4,2%	5,2%	4,3%	5,0%	4,0%	4,7%	5,9%	6,5%	4,4%	3,5%	4,3%	3,7%	4,1%	3,5%	4,6%	4,5%	

Table A3

Sample no.	Lab. no.	No. of crystals analysed	He no.	⁴ He (ncc)	Th/U ratio	^a Mean F _T	Age (Ma)	Error ($\pm 2\sigma$) (Ma)
21	8971	3	27059	0,047	11,86	1,00	0,69	0,04
21	9009	4	27145	0,078	12,88	1,00	0,89	0,05
21	9069	7	27193	0,166	12,26	1,00	0,58	0,03
21	9070	6	27195	0,208	13,29	1,00	0,57	0,03
21	11669	4	36352	0,035	15,75	1,00	0,65	0,04
							^b 0,65	^b 0,13
25	8989	1	27083	0,017	13,34	1,00	0,64	0,04
25	9012	6	27156	0,044	8,82	1,00	^c 1,33	0,08
25	11673	4	36364	0,075	11,60	1,00	0,63	0,04
25	11674	6	36367	0,029	11,39	1,00	0,76	0,05
25	9072	5	27199	0,068	11,35	1,00	0,62	0,04
							^b 0,66	^b 0,09
<i>Durango apatite - standard</i>								
Durango	9074	1	27204	1,308	17,32	1,00	32,4	2,0
Durango	11658	1	36180	5,357	15,27	1,00	31,6	2,0
Durango	11675	1	36289	3,867	15,18	1,00	31,7	2,0
Durango	11684	1	36400	21,672	17,25	1,00	29,7	1,8
							^b 31,3	^b 1,9

^a FT is the a-ejection correction after Farley et al. (1996).

^b Weighted mean ages (95% confidence level) calculated using Isoplot v. 3.0 (Ludwig, 2003).

^c Analysis excluded from calculation of weighted mean.

Table A4

Phlogopite						Fluorapatite				Clinopyroxene								
Sample	Initial (2M)			Separated-1 (0.5M)			Separated-2 (2M)			AC-21	AC-24	AC-25	AC-21	AC-24	AC-25	AC-21	AC-24	AC-25
	ppm	AC-21	AC-24	AC-25	AC-21	AC-24	AC-25	AC-21	AC-24	AC-25	AC-21	AC-24	AC-25	AC-21	AC-24	AC-25	AC-21	AC-24
Rb	431	169	66	513	475	409	210	378	459	0,3	0,4	2,6	4,2	0,1	11			
Sr	1672	3748	236	115	227	196	118	174	169	5830	6335	3114	469	203	452			
Rb/Sr	0,26	0,05	0,28	4,48	2,09	2,08	1,79	2,18	2,72	0	0	0,001	0,009	0	0,024			
⁸⁷ Rb/ ⁸⁶ Sr	0,7458	0,1301	0,8143	12,9521	6,0468	6,0261	5,1638	6,2915	7,8585	0	0	0,002	0,026	0,001	0,068			
⁸⁷ Sr/ ⁸⁶ Sr	0,703471	0,703463	0,703475	0,70397	0,70338	0,70343	0,70346	0,70345	0,70331	0,70337	0,70346	0,70354	0,70353	0,70311	0,70309			

Table A5

Lambda 5,54E-10													Regression								
	Sample #	$^{40}\text{Ar}/^{39}\text{Ar}$	E(%) (1s)	J-value	E(%, 1s)	Age (Ma)	E (%)	Error (excl.) 1s	Error (incl.) 1s	E (%)	Error (excl.) 2s	Error (incl.) 2s	E (Ma)	$^{40}\text{Ar}/^{36}\text{Ar}$	E(%) (1s)	E(%) (2s)	MSWD	p	n	uncert. type (1σ or 95%CI)	
21PHL																					
Total gas ages																					
21PHL-1	21PHL-1	3.44	13.82	0.000105027	0.036	0.652	13.821	0.090	13.821	0.090	27.643	0.180									
21PHL-2	21PHL-2	3.89	6.11	0.000105027	0.036	0.737	6.111	0.045	6.111	0.045	12.223	0.090	12.222	0.090							
21PHL-3	21PHL-3	4.48	15.79	0.000105027	0.036	0.848	15.791	0.134	15.791	0.134	31.582	0.268	31.582	0.268							
21PHL-4b	21PHL-4b	3.49	9.75	0.000105027	0.036	0.660	9.744	0.064	9.744	0.064	19.488	0.129	19.488	0.129							
21PHL-5b	21PHL-5b	2.74	35.84	0.000105027	0.036	0.519	35.835	0.186	35.835	0.186	71.669	0.372	71.669	0.372							
Inverse isochron results																					
21PHL-1, steps 1-6		4.15	6.22	0.000105027	0.036	0.786	6.223	0.049	6.223	0.049	12.446	0.098	12.445	0.098	297.59	0.12	0.37	0.74	0.66	0.62	6
21PHL-1,2,3,4,5 n=12 (non rejected (red) points)		4.03	4.23	0.000105027	0.036	0.764	4.233	0.032	4.233	0.032	8.466	0.065	8.466	0.065	298.18	0.08	0.23	0.46	1.7	0.07	12
21PHL-1,2,3,4,5 n=6 (concordant (bold) steps)		4.12	5.14	0.000105027	0.036	0.780	5.143	0.040	5.143	0.040	10.286	0.080	10.286	0.080	298.18	0.13	0.38	0.75	1.4	0.21	7
Weighted mean age of 5 grains (high-T concordant points, n=7)	(PREFERRED AGE FOR 21PHL)	3.91	2.95	0.000105027	0.036	0.741	2.950	0.022	2.949	0.022	5.899	0.044	5.899	0.044					1.3	0.23	7
24PHL, 25PHL																					
Inverse isochron results																					
24PHL- Grain 1&2 (n=3)		2.92	2.19	0.000104856	0.037	0.552	2.188	0.012	2.188	0.012	4.376	0.024	4.375	0.024	302.15	0.18	0.55	0.2	0.65	3	2s
24PHL- Grain 1&2 + 25PHL (n=6)		2.95	1.91	0.000104685	0.037	0.556	1.915	0.011	1.914	0.011	3.829	0.021	3.829	0.021	302.01	0.14	0.44	0.5	0.73	6	2s
Total gas ages																					
Sample 24PHL-2		4.22	5.12	0.000104856	0.037	0.797	5.119	0.041	5.119	0.041	10.238	0.082	10.238	0.082	9.236	0.063	0.063	1,09555			
Sample 25PHL-1		3.63	4.62	0.000104685	0.037	0.686	4.618	0.032	4.618	0.032	9.236	0.063	9.236	0.063							

Table A6

Sample <i>ppm</i>	Groundmass			Clinopyroxene			Fluorapatite		
	AC-21	AC-24	AC-25	AC-21	AC-24	AC-25	AC-21	AC-24	AC-25
Rb	4.17	5.05	8.75	6.2	0.3	95.2	0.04	0.18	0.6
Sr	2495	2442	1036	601	146.6	2861	3539	4274	3996
Nd	220	211	183	40.6	21.4	16.27	536	1155	839
Sm	28	27.1	22.3	11.3	6.06	37.97	163	169	123.4
Lu	0.32	0.32	0.24	0.18	0.08	0.42	1.08	1.08	0.8
Hf	2.94	3.1	2.95	20.35	17.11	61.86	0.09	0.29	0.16
Pb	2.34	1.37	2.74	0.48	0.36	1.75	0.97	221.2	0.97
Th	18.5	18.4	14.1	0.68	0.23	1.18	50.62	92.9	54.91
U	6.77	6.43	4.97	0.13	0.04	0.31	3.88	6.53	4.59
$^{87}\text{Rb}/^{86}\text{Sr}$	0.00482	0.00597	0.02441	0.02987	0.0059	0.09618	0.00003	0.00012	0.00045
$^{87}\text{Sr}/^{86}\text{Sr}$	-	-	-	0.70353	0.70310	0.70309	0.70336	0.70346	0.70354
$^{147}\text{Sm}/^{144}\text{Nd}$	0.07708	0.07762	0.07388	0.10131	0.10911	0.12269	0.08968	0.08851	0.08868
$^{143}\text{Nd}/^{144}\text{Nd}$	0.51279	0.51282	0.51280	0.51280	0.51286	0.51281	0.51278	0.51278	0.51278
ϵNd	2.96	3.47	3.08	3.22	4.23	3.36	2.81	2.85	2.83
$^{176}\text{Lu}/^{177}\text{Hf}$	0.01546	0.01466	0.01155	0.00090	-	0.00081	-	-	-
$^{176}\text{Hf}/^{177}\text{Hf}$	0.28280	0.28281	0.282802	0.28275	-	0.28283	-	-	-
ϵHf	1.20	1.24	1.06	-0.71	-	1.95	-	-	-
$^{238}\text{U}/^{204}\text{Pb}$	193	314.24	120.3	-	-	-	261.17	-	-
$^{232}\text{Th}/^{204}\text{Pb}$	547	930.66	353.64	-	-	-	3584.62	-	-
$^{206}\text{Pb}/^{204}\text{Pb}$	20.58	20.5	20.09	-	-	-	20.5	-	-
$^{207}\text{Pb}/^{204}\text{Pb}$	15.79	15.81	15.78	-	-	-	15.81	-	-
$^{208}\text{Pb}/^{204}\text{Pb}$	39.99	40.17	39.87	-	-	-	40.18	-	-